Blur grey-level hit-or-miss transform for fully automatic 3D segmentation of coronary arteries

Bessem Bouraoui, Christian Ronse, Nicolas Passat, Joseph Baruthio, Philippe Germain

Blur grey-level hit-or-miss transform for fully automatic 3D segmentation of coronary arteries

B. Bouraoui*, C. Ronse, N. Passat
LSIIT UMR 7005 CNRS-ULP, France

J. Baruthio
LINC UMR 7191 CNRS-ULP, France

Ph. Germain
Service de Radiologie, CHU Strasbourg, France

Abstract

3D CT scan images of coronary arteries are complex to analyze because they provide a 3D object that is visualized through 2D projections. Medical diagnosis suffers from inter- and intra-clinician variability. Therefore, reliable software for the 3D reconstruction and labeling of the coronary tree is strongly desired [4]. Finding appropriate methods is known to be a challenging problem because of data imperfections: noise, heterogeneous intensity [14]...

In this paper we propose a fully automatic algorithm for coronary artery extraction from X-ray data sequences of a cardiac cycle (3D-CT scan, 64 detectors, 10 phases) introduced in [2, 3].

Our method is based on the blur grey-level HMT, and it is guided by anatomical knowledge. Our segmentation gives good result on 90% of the images, while those where it fails are very noisy. It is therefore a promising tool for the automatic 3D reconstruction of the coronary tree from $3D$ temporal angiographic sequences.

Index Terms— coronary arteries, segmentation, anatomical knowledge, hit-or-miss transform, region-growing.

1 Introduction

Vessel segmentation algorithms are the key components of automated radiological diagnosis systems. Segmentation strategies vary depending on the imaging modality, application domain, automation requirements, and other specific factors [13, 6]. Most image processing concepts have been involved in the development of segmentation methods for coronary arteries. Among them, mathematical morphology is one of the most recently considered approaches [2, 3], following its successful application to the segmentation of hepatic [9, 10] and cerebral [12, 11] vascular networks.

In this paper we propose an extension of a morphological operator, to improve a fully automatic method of segmentation of the coronary arteries in large X-ray images [2, 3]. Processing images which may be noisy and present variable contrasts between the different acquisitions [7], the main idea of this extension is to make these differences from an image to another minimized. Our results have been validated by an expert.

*bouraoui@lsiit.u-strasbg.fr

2 Background

We used a large anatomical knowledge. In [2, 3] two methodologies are combined: an improved grey-level hit-or-miss transform, and region-growing. The segmentation is performed in three steps. The same steps are considered in this paper, but applied in another way, using a new morphological operator.

Region-growing methods are based on two main concepts: seed-point(s) and expansion criterion. Starting from the seed-point(s), and iteratively exploring - until stability - the currently segmented object neighborhood, if the expansion criterion is satisfied for a given point, this point is added to the object, see [2, 3].

3 Hit-or-miss transform

Formally, the binary HMT transform by the pair (A, B) associates to a binary image X the set $X \otimes (A, B)$ of positions where the translate of A fits inside X and at the same time the translate of B fits inside the complement X^c of X:

$$\begin{aligned} X \otimes (A, B) &= \{p \in E \mid A_p \subseteq X,\ B_p \subseteq X^c\} \\ &= (X \ominus A) \cap (X^c \ominus B)\ . \end{aligned} \tag{1}$$

For the grey-level HMT operator, we use a definition [8] that assigns to A and B grey-levels a and b, respectively. Following this definition, the grey-level (GL) HMT compares at each point p the minimum intensity a_{min} in A_p to the maximum intensity b_{max} in B_p:

$$S_s^t = I_s \otimes (A, B)(p) = \begin{cases} (I_s \ominus A)(p) - a & \text{if } (I_s \ominus A)(p) - a \\ & \geq (I_s \oplus \check{B})(p) - b\ , \\ \bot & \text{otherwise}\ . \end{cases} \tag{2}$$

If $a_{min} > (b_{max} + a - b)$, then the point is selected by the GL HMT. An example of HMT is illustrated in Fig. 1.

4 Blur hit-or-miss transform

Although the HMT is sensitive to the types of noise found in scanned images, including both boundary and random

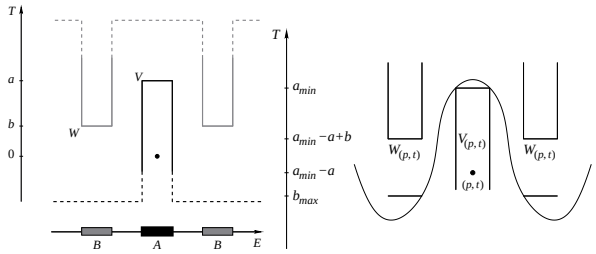

Figure 1: Left: The foreground structuring function V has value a on A and and $-\infty$ elsewhere, while the background structuring function W has value b on B and $+\infty$ elsewhere. Right: Given a_{min}, the minimum grey-level of I in A_p and b_{max}, the maximum grey-level of I in B_p, we have $a_{min} - a + b \geq b_{max}$, so the point p is selected with grey-level $a_{min} - a$.

noise, a simple extension, the blur HMT, is relatively robust. The noise immunity of the blur HMT derives from its ability to deal with both types of noise together, and to remove them by appropriate dilation or erosion. Thus the blur HMT (B HMT) can be used as a fast heuristic to avoid more expensive integer-based matching techniques, and it is implemented efficiently with morphological image operators.

The blur binary hit-or-miss transform (BB HMT) was introduced in [1]. In the binary HMT, cf. (1), a point p may not belong to $X \otimes (A, B)$ because of small holes or narrowings in X or X^c, due to noise. They can be eliminated by dilating the foreground X and background X^c by two structuring elements G and H that depend on image noise and pattern variability. Thus we compute

$$\begin{aligned} & X \otimes (A, B; G, H) \\ & = \{p \in E \mid A_p \subseteq X \oplus G \text{ and } B_p \subseteq X^c \oplus H\} \\ & = \big((X \oplus G) \ominus A\big) \cap \big((X^c \oplus H) \ominus B\big) \\ & = \big((X \oplus G) \ominus A\big) \setminus \big((X \ominus \check{H}) \oplus \check{B}\big) \ . \end{aligned} \tag{3}$$

In the grey-level case, the dilation of the dark background is obtained by eroding the image. Here G and H are flat structuring elements. Thus we compute for an image I the following blur GL HMT (B GL HMT):

$$\eta^S_{[V,W;G,H]}(I)(p) = \begin{cases} \big[(I \oplus G) \ominus A\big](p) - a & \text{if } \big[(I \oplus G) \ominus A\big](p) - a \\ & \geq \big[(I \ominus \check{H}) \oplus \check{B}\big](p) - b \ , \\ \perp & \text{otherwise} \ . \end{cases} \tag{4}$$

Indeed, the dilation $I \oplus G$ eliminates dark noise in the bright foreground while the erosion $I \ominus H$ eliminates bright noise in the dark background. Often one can take the two smoothing structuring elements equal, $G = H$, and symmetrical, $\check{G} = G$.

In this paper, we will apply the B GL HMT to low quality 3D grey-level images obtained from heart scanners of several patients.

5 Segmentation method — Application on the coronary arteries

The method requires as input a 4D X-ray image covering the cardiac cycle on ten phases. The coronary arteries do not introduce the same contrast and dimension on all stages of the cardiac cycle. An optimum choice of the phases proves to be necessary. During the diastole, the coronary arteries are the most dilated, so they present a better size and contrast in that stage. The diastole corresponds to the 7^{th}, 8^{th} and 9^{th} phases of the 4D image. We are therefore going to choose these three phases to search the coronary arteries, and keep the best segmentation.

Selecting one of these phases of the heart, we obtain a 3D image I which can be considered as a function $I : E \to Z$ (with $E = [0, 511]^3$), associating to each point $x \in E$ its grey-level $I(x)$ in the image. Since the method is fully automatic, no other parameter is required. The method provides as output a binary image $S \subset E$ corresponding to the segmented coronary arteries detected in I.

The heart zone is detected in the same way as in [2, 3], the image I has huge dimensions so a sub-sampling is applied. Here we don't need a blur HMT, only an ordinary GL HMT is applied. The idea was then to use a GL HMT on a subsampled image, considering the lungs as background and the heart as object. The GL HMT (2) results in a subset $S^h_s \subset E_s = [0, 127]^3$, which corresponds to the heart region (Fig. 2 Right). Then an over-sampling followed by an AND with the original image, allows to come back to the original size (512^3). A over-sampled version S^a of S^a_s is then obtained as $S^a = \bigcup_{x \in E}(4.x + [0, 3]^3)$.

As result, the search zone is reduced to one third comparing to the original size, and then we can start the coronary arteries segmentation.

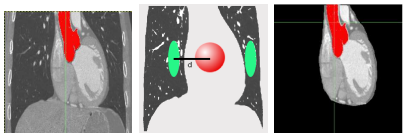

Figure 2: Heart zone detection. Left: Original image. Middle: Structuring element used for the heart zone detection. Right: Heart zone.

The pre-processing (illustrated in Fig. 3) consists in the detection of the heart zone followed by filtering the images, to produces two new images: I_B for the background freed from "salt" noise, and I_F for the foreground freed from "pepper" noise. We use a filter with a window forming a 4^3-cube; for I_B we keep the lowest intensity, $I_B(x) = \min\{I(y) \mid y \in x + [0, 3]^3\}$, while for I_F we keep the highest intensity, $I_F(x) = \max\{I(y) \mid y \in x + [0, 3]^3\}$. Then we erode I_B and dilate I_F, as required by the blur GL HMT, see (4). Thus we apply the GL HMT, cf. (2), with two images instead of only one: at each location, the foreground structuring element has to fit in I_F and the background structuring element has to fit in I_B; if the difference of grey-levels $a_{min} - b_{max}$ exceeds the required minimum

$a - b$, the point is selected. This application of the blur GL HMT (B GL HMT) is slightly more complicated than in theory (4).

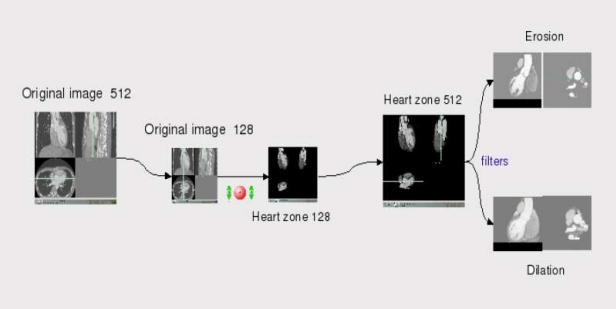

Figure 3: Image pre-processing.

Starting from the previously obtained subset S_s^h (corresponding to the heart region) we create a new subset S_s^a representing the aorta. Our goal is to locate this circular shape using a B GL HMT with multi-sized structuring elements. A horizontal disk A with a variable radius models the object. To model the background, we surround this disk with 8 points regularly sampled on a discrete circle B (Fig. 4 Right).

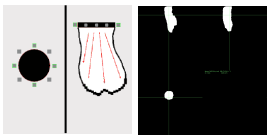

Figure 4: Aorta Segmentation. Left: Structuring elements for the circular axial section detection. Right: The aorta.

It is easy to notice that in the original image, the dark space where the background structuring element should fit is relatively narrow, thus the pre-processing performed above (Fig. 3: Right) would allow to widen this region before we apply the B GL HMT using the structuring elements in Fig. 4: Left. Once this circular shape is detected, we calculate the average value of the intensities on this cut. The center of the detected circular shape will be used as seed for a first region-growing, the expansion criterion of which will involve two parameters: intensity thresholding and variance [5], and will evolve in the direction of the beginning of the aorta, stopped by the aorta wall on the sides and by the aortic valve below (Fig. 4: Middle). The B GL HMT followed by the region-growing results in the subset $S_s^a \subset S_s^h$ which corresponds to the aorta segment.

The coronary arteries are the only tubular structures that arise from the beginning of the aorta. The idea is to search them in the wall of the aorta. Following a strategy close to the one proposed in [9, 10], a B GL HMT is applied, with a sphere as object and 8 points surrounding this sphere as background. These points belong to the plane normal to the artery axis. The choice of these points defines the axis direction of the searched coronary artery. Thus 13 structuring elements, corresponding to the 13 discrete principal directions, are used (Fig. 5: Left).

This B GL HMT is applied on the aorta wall, thus we obtain two seed-points $S_l = (x_l, y_l, z_l)$ and $S_r = (x_r, y_r, z_r) \in S^a$ for the left and right artery coronaries.

Figure 5: Coronary arteries segmentation. Left: Structuring element used for the coronary arteries detection. Middle: Results of the B GL HMT. Right: Results of the Adaptive B GL HMT.

Starting from the two seed-points S_r and S_l previously detected on the aorta wall, a region-growing is performed, applying the B GL HMT on every neighbor as criterion. The involved structuring elements are the same as those described above for the seed-point detection. The result is a subset $S \subset E$ which corresponds to the coronary arteries. An example of result (aorta and coronary arteries) is illustrated in Fig. 5: Middle.

Using the B GL HMT with a fixed grey-level difference between the foreground and the background, does not allow the region growth to go far enough in the arteries. The more we advance in the coronary arteries, the darker they become, because of their decreasing size and the lower concentration of the injected contrast product. In the small bifurcations they have a contrast with the cardiac muscle which is less important than at the beginning of the artery.

An adaptive application of the B GL HMT during the region growing is necessary, in order to detect the greatest part of this artery. The adaptive aspect will consist in the reduction of the grey-level difference defined in the B GL HMT; during the region growth, each time that the B GL HMT fails, this difference is reduced by a small amount, while the structuring elements keep the same geometric form. This region growth stops when after 2 successive reductions of the difference, the B GL HMT still fails.

We have thus applied an Adaptive B GL HMT, that gives a better results and makes the method more efficient (Fig. 5: Right).

We summarize here our algorithm, it is also illustrated in Fig. 7.

Input: Original image: $I : E \rightarrow Z$ with 512^3 size.

- Pre-processing:
  - Under-sampling to get a 128^3 image: $I_s(x) = \min\{I(y) \mid y \in 4.x + [0,3]^3\}$.
  - Heart zone detection by GL HMT application: $S_s^h \subset E_s$.
  - High intensity filter application and dilation to get: $I_F(x) = \max\{I(y) \mid y \in x + [0,3]^3\}$ dilated.
  - Low intensity filter application and erosion to get: $I_B(x) = \min\{I(y) \mid y \in x + [0,3]^3\}$ eroded.
- Coronary arteries segmentation.
  - Aorta segmentation: $S_s^a \subset E$.

    - ∗ Circular coronal section localization.
    - ∗ Calculate the average intensity on this coronal section.
    - ∗ Region-growing starting by the circular shape center and using the calculated average intensity as criterion, in the direction of the beginning of the aorta.
  - Over-sampling of the aorta to a 512^3 image: $I^a \subset E_s$.
  - Search of the two coronary arteries seed-points on the aorta wall: S_r and S_l.
  - Coronary arteries detection with a region-growing using the Adaptive B GL HMT as criterion: $S \subset E$.

Output: Coronary arteries 512^3 image: I^c.

Figure 6: Example of segmented image: Left: faulty image; Middle: without post-processing; Right: with post-processing.

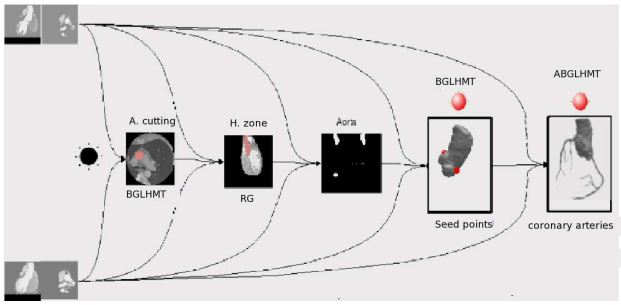

Figure 7: Method application.

6 Experiments and results

The method was tested on 60 coronal scan images, for the 3 chosen phases of 20 patients, providing visually satisfactory results. The first part of the method (the heart zone detection) has been validated on 20 other patients. In this method, some dimensions had to be set, like the radius of the horizontal disk in the aorta detection. Several radiuses were tried on a set of images, and for each image the best radius was selected. We obtained thus a range of radiuses for the whole base. This allows to us adjust the radius to each image of the base.

We can separate our results into three groups. A first group composed of 50% of the tested images gives satisfactory results. A second group composed of 40% of the images provides less satisfactory results, the region growth in the last step (for segmenting the coronary arteries) has been diverted to give false positives, in most cases consisting of the wall of the heart. Thus a post-processing of this group of images becomes necessary, it consists in adding a constraint on the GL HMT, namely the percentage of accepted voxels in the object structuring element, we require 90% of these voxels to satisfy the difference of grey-level between them and the maximum grey-level of the background (Fig. 6); note that this added constraint has no effect on the first group of images that already had satisfactory results. The last group consists of the remaining 10% images, they are noisier and their variance is higher than that of the others; thus some of the coronary arteries in these images are completely blurred and present no contrast with the background, which makes the application of the fully automatic segmentation just impossible Fig. 6.(1).

Finally we got satisfactory results for 90% of our image base validated by an expert cardiologist.

References

[1] D. Bloomberg and L. Vincent. Pattern matching using the blur hit-miss transform. *Journal of Electronic Imaging*, 9(2):140–150, 2000.

[2] B. Bouraoui, C. Ronse, J. Baruthio, N. Passat, and Ph. Germain. Gray-level hit-or-miss transform based region-growing for automatic segmentation of 3D coronary arteries. In *International Symposium on Mathematical Morphology 2007, Proceedings*, volume 2, pages 23–24, 2007.

[3] B. Bouraoui, C. Ronse, J. Baruthio, N. Passat, and Ph. Germain. Fully automatic 3D segmentation of coronary arteries based on mathematical morphology. In *ISBI 2008, 5th International Symposium on Biomedical Imaging: From Nano to Macro*, pages 1059–1062. IEEE, may 2008.

[4] C. Chalopin, G. Finet, and I. E. Magnin. Modeling the 3d coronary tree for labeling purposes. *Med Image Anal*, 5:301–315, Dec 2001.

[5] J. Fleureau, M. Garreau, A.I. Hernández, A. Simon, and D. Boulmier. Multi-object and N-D segmentation of cardiac MSCT data using SVM classifiers and connectivity algorithm. In *Computers in Cardiology 2006, Proceedings*, volume 33, pages 817–820, 2006.

[6] C. Kirbas and F. Quek. A review of vessel extraction techniques and algorithms. *ACM Computing Surveys*, 36(2):81–121, 2004.

[7] C. Lorenz, S. Renisch, T. Schlatholter, and T. Bulow. Simultaneous segmentation and tree reconstruction of the coronary arteries in MSCT images. *SPIE Medical Imaging: Physiology and Function: Methods, Systems, and Applications 2003, Proceedings*, 5031:167–177, 2003.

[8] B. Naegel, N. Passat, and C. Ronse. Grey-level hit-or-miss transforms - Part II: Application to angiographic image processing. *Pattern Recognition*, 40(2):648–658, February 2007.

[9] B. Naegel, C. Ronse, and L. Soler. Segmentation automatique de l'entrée de la veine porte dans le foie par application de la transformée en tout-ou-rien en niveaux de gris. In *ORASIS 2003, 9e congrès, Proceedings*, pages 33–37, Gérardmer, France, May 2003.

[10] B. Naegel, C. Ronse, and L. Soler. Using grey-scale hit-or-miss transform for segmenting the portal network of the liver. In C. Ronse, L. Najman, and E. Decencière, editors, *Mathematical Morphology: 40 years on. Proceedings of the 7th International Symposium on Mathematical Morphology*, volume 30 of *Computational Imaging and Vision*, pages 429–440, Paris, France, April 2005. Springer SBM.

[11] N. Passat, C. Ronse, J. Baruthio, J.-P. Armspach, and C. Maillot. Magnetic resonance angiography: From anatomical knowledge modeling to vessel segmentation. *Medical Image Analysis*, 10(2):259–274, 2006.

[12] N. Passat, C. Ronse, J. Baruthio, J.-P. Armspach, C. Maillot, and C. Jahn. Region-growing segmentation of brain vessels: An atlas-based automatic approach. *Journal of Magnetic Resonance Imaging*, 21(6):715–725, 2005.

[13] J.S. Suri, K. Liu, L. Reden, and S. Laxminarayan. A review on MR vascular image processing: Skeleton versus nonskeleton approaches: Part II. *IEEE Transactions on Information Technology in Biomedicine*, 6(4):338–350, 2002.

[14] A. Szymczak, A. Stillman, A. Tannenbaum, and K. Mischaikow. Coronary vessel trees from 3d imagery: a topological approach. *Medical Image Analysis*, 10:548–559, 2006.